

Elastic scattering of the unstable nucleus ${}^7\text{Be}$ on ${}^{12}\text{C}$ at 140 MeV

T. Yamagata and K. Yuasa

Department of Physics, Konan University, Higashinada, Kobe 658, Japan

N. Inabe and M. Nakamura

Department of Physics, Kyoto University, Kyoto 606, Japan

M. Tanaka

Kobe Tokiwa Junior College, Nagata, Kobe 653, Japan

S. Nakayama

College of General Education, Tokushima University, Tokushima 770, Japan

K. Katori

Laboratory of Nuclear Studies, Osaka University, Toyonaka, Osaka 560, Japan

M. Inoue

Keage Laboratory, Institute for Chemical Research, Kyoto University, Kyoto 606, Japan

S. Kubono

Institute for Nuclear Study, University of Tokyo, Tanashi, Tokyo 188, Japan

T. Itahashi and H. Ogata

Research Center for Nuclear Physics, Osaka University, Ibaraki, Osaka 567, Japan

Y. Sakuragi

Department of Physics, Osaka City University, Sumiyoshi, Osaka 558, Japan

(Received 25 October 1988)

The first data of elastic scattering of the unstable nucleus, ${}^7\text{Be}$ ($T_{1/2} = 53.3$ d), are presented for a ${}^{12}\text{C}$ target at 140 MeV. Secondary beams of ${}^7\text{Be}$ were produced by using a polyethylene target with the reaction of ${}^1\text{H}({}^7\text{Li}, {}^7\text{Be})$ at $\theta_{\text{lab}} = 0^\circ$. A magnetic spectrograph was used to focus ${}^7\text{Be}$ particles ejected from the polyethylene target onto a carbon target. The beam-spot size at the carbon target was less than $2\text{ mm} \times 2\text{ mm}$. The energy resolution of ${}^7\text{Be}$ beams was 1.6 MeV (full width at half maximum) with intensity of $2 \times 10^4\text{ s}^{-1}$. Data were analyzed in terms of the double-folding model. It was found that a 25% reduction in the real-potential strength is required to fit the experimental cross section. Coupled-channel calculations demonstrated that such a reduction is due to the effect of projectile breakup.

I. INTRODUCTION

Unstable nuclei have some different properties from stable ones; spin, isospin, or nuclear radii, etc.¹ Therefore experiments with unstable nuclear beams are of great interest for the study of nuclear structure and nucleus-nucleus interactions.

We have succeeded in producing secondary beams of monoenergetic ${}^7\text{Be}$ ($T_{1/2} = 53.3$ d) at an intermediate energy region ($E/A \sim 20$ MeV). In this paper we present results and analyses of elastic scattering undertaken by this ${}^7\text{Be}$ beam.

Recently, considerable attention has been paid to the role of projectile breakup processes in nuclear reactions.² Since cross sections of the projectile breakup reactions are very large, these processes modify the cross sections among various reaction channels. Particularly, in elastic

scattering of light heavy ions with clustering structures significant effects of the breakup processes have been pointed out.^{3,4} For ${}^{6,7}\text{Li}$ nuclei it was found that the usual folding model failed to reproduce angular distributions of elastic scattering and a large reduction in strength should be required for the folding potentials to fit the elastic scattering data.⁵ This conclusion was contrasted with the case obtained for other projectiles, whose elastic scattering was successfully predicted with the folding model.⁵ This seemed mainly due to low threshold energies of ${}^{6,7}\text{Li}$ for the projectile breakup into two clusters. According to the theoretical analysis such a reduction was really attributed to a dynamic repulsive potential induced by the breakup effect of the projectiles on the elastic channel.^{4,6}

It is very interesting to confirm whether this physical picture is valid also for projectiles other than Li ions or

not. For this purpose, the ${}^7\text{Be}$ projectile seems to be an appropriate candidate because the threshold energy for the breakup reaction into ${}^3\text{He} + \alpha$ is low (1.59 MeV). Furthermore, since ${}^7\text{Be}$ is a mirror nucleus of ${}^7\text{Li}$, the theoretical treatment involves little ambiguity between ${}^7\text{Be}$ and ${}^7\text{Li}$. Based on the above aspect we measured elastic scattering of ${}^7\text{Be}$ on ${}^{12}\text{C}$ at an incident energy of 140 MeV. Experimental differential cross sections were analyzed in terms of the double-folding model, in which projectile breakup processes were explicitly taken into account along with the so-called method of coupled discretized continuum channel (CDCC).⁴

II. EXPERIMENTAL PROCEDURE AND RESULTS

The present experiment was essentially a sort of double scattering, very similar to previous work:⁷ ${}^7\text{Be}$ particles were produced from a ${}^1\text{H}({}^7\text{Li}, {}^7\text{Be})$ reaction and then scattered by a carbon target. Since the cross section of this reaction was found to be large [$\sigma_{\text{lab}}(0^\circ) \sim 0.5$ b/sr] in our previous work⁸ intense ${}^7\text{Be}$ beams were expected to be possibly obtained with a thin target, which was required for a good energy resolution. Figure 1 shows an experimental setup. 147-MeV ${}^7\text{Li}^{3+}$ beams were provided from the azimuthally veering field (AVF) cyclotron at the Research Center for Nuclear Physics (RCNP), Osaka University. Beams were transported with an achromatic mode and focused on a polyethylene target of 8 mg/cm² thickness, positioned at the center of the first scattering chamber of the magnetic spectrograph, "DUMAS."⁹ A laboratory angle of the DUMAS was set at 0°. ${}^7\text{Li}$ beams passing through the polyethylene target were introduced into the DUMAS and were collected by a Faraday cup attached on a side wall of a vacuum chamber of the DUMAS. A typical ${}^7\text{Li}$ beam intensity and an energy resolution were 20 nA and 500 keV, respectively. ${}^7\text{Be}$ particles

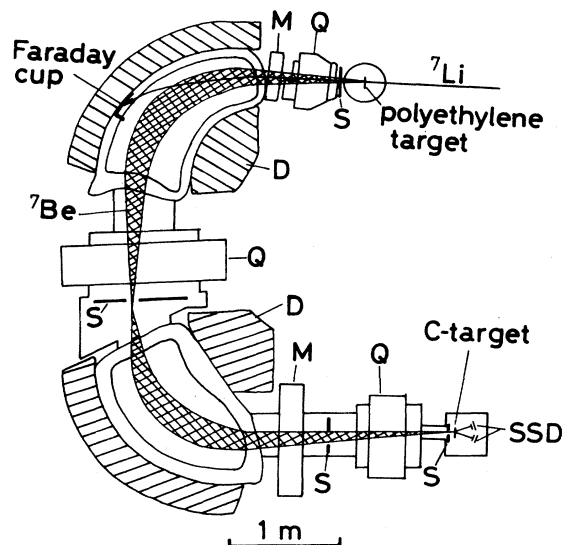


FIG. 1. Experimental setup. *D*, *Q*, *M*, and *S* denoted in the figure are a dipole, a quadrupole, a multipole magnet, and a slit, respectively. An envelope of ${}^7\text{Be}$ beams is shown with a crossed area.

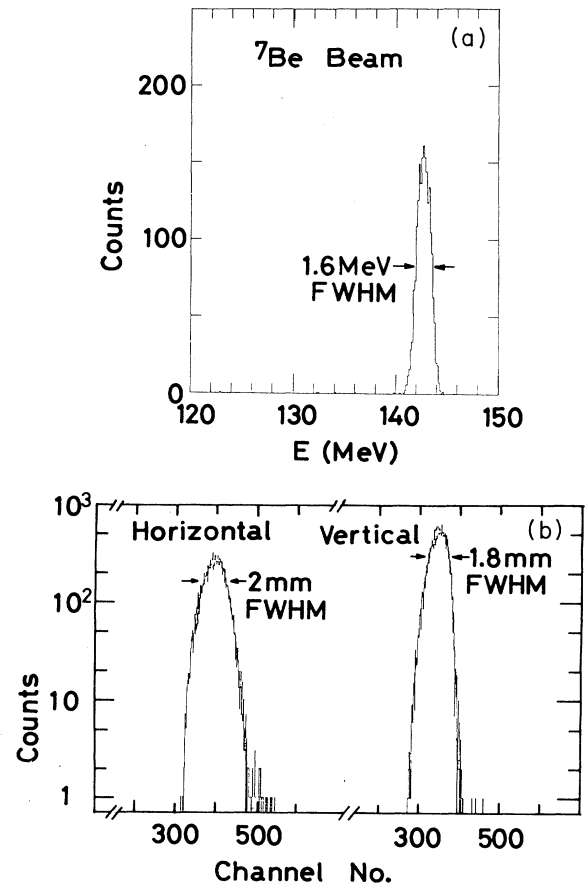


FIG. 2. (a) An energy and (b) position spectra of incident ${}^7\text{Be}$ beams at the carbon target position.

from a ${}^1\text{H}({}^7\text{Li}, {}^7\text{Be})$ reaction emitted in angular ranges of $|\theta_{\text{lab}}| \leq 1^\circ$ and $|\phi_{\text{lab}}| \leq 1^\circ$ were accepted and focused by the DUMAS onto a carbon (${}^{\text{nat}}\text{C}$) target of 18 mg/cm² thickness, mounted at the center of the second scattering chamber.⁷ An incident energy of ${}^7\text{Be}$ was 144 MeV and an energy loss of ${}^7\text{Be}$ through the carbon target was 7

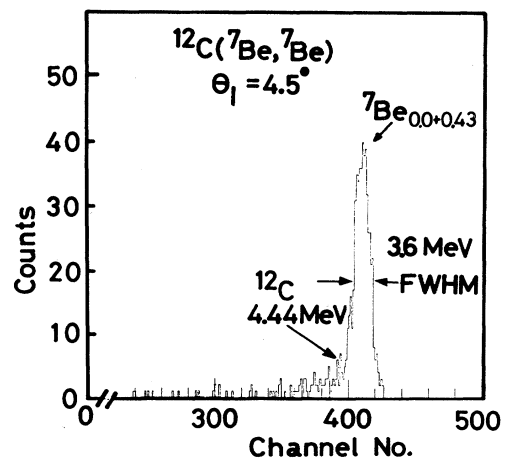


FIG. 3. An energy spectrum of ${}^7\text{Be}$ particles scattered by the carbon target at $\theta_{\text{lab}} = 4.5^\circ$.

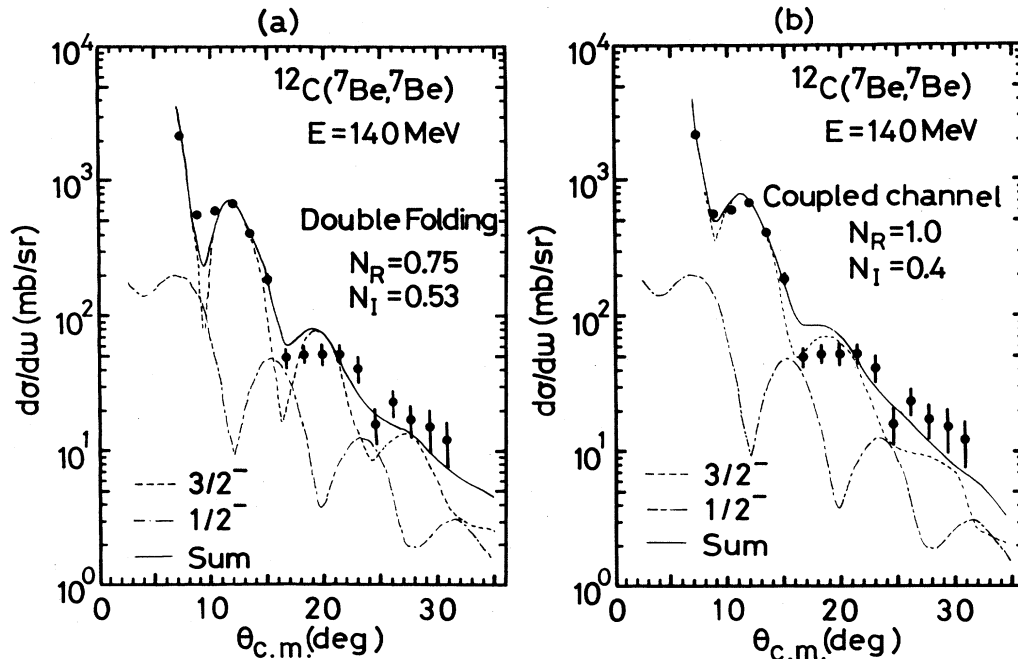


FIG. 4. Experimental and calculated differential cross sections. (a) Double-folding and (b) coupled-channel calculations. Broken and dotted chain lines show calculated results for the ground state and the $\frac{1}{2}^-$ state transitions, respectively. A sum of these is shown by a solid line.

MeV. We estimated a mean energy of ${}^7\text{Be}$ averaged over the target thickness to be 140 MeV.

At the position of the carbon target a position sensitive Si detector was additionally mounted for ${}^7\text{Be}$ beam diagnostics during a tuning of the DUMAS. Figure 2 shows energy and position spectra of incident ${}^7\text{Be}$ beams measured with this detector. An energy spreading [full width at half maximum (FWHM)] was 1.6 MeV, mainly determined by a difference of an energy loss between ${}^7\text{Li}$ and ${}^7\text{Be}$ ions in the polyethylene target. A beam-spot size at the carbon target was less than $2 \times 2 \text{ mm}^2$. Angular divergences of the ${}^7\text{Be}$ beam were measured to be $\pm 0.1^\circ$ and $\pm 1.3^\circ$ in a horizontal and a vertical direction, respectively. With this setup, a typical intensity of ${}^7\text{Be}$ beams was $2 \times 10^4 \text{ s}^{-1}$. Impurities in ${}^7\text{Be}$ beams were mainly α , ${}^6\text{Li}$, and ${}^7\text{Li}$ particles. Intensities of these particles were about 0.5, 0.1, and 0.1 times the ${}^7\text{Be}$ intensity, respectively, and their energies were 60, 90, and 80 MeV, respectively. Therefore no problem was caused by these low intensities and low energy impurities in the present measurement.

Scattered ${}^7\text{Be}$ particles were detected in an angular range of $4^\circ \leq \theta_{\text{lab}} \leq 20^\circ$ by several runs using two sets of position sensitive Si-detector telescopes consisting of 500- μm -thick ΔE and 5-mm E detectors. In this measurement we made sure that each angular region of the detectors sufficiently overlapped the other. Figure 3 shows a typical energy spectrum of ${}^7\text{Be}$ particles scattered by the carbon target. An observed energy resolution was 3.6 MeV (FWHM), mainly due to an energy straggling of ${}^7\text{Be}$ in the carbon target. The ground state peak was separated from the 2^+ peak in ${}^{12}\text{C}$ at $E_x = 4.44 \text{ MeV}$, as seen in Fig. 3. On the other hand, the peak of

$E_x = 0.43 \text{ MeV}$ in ${}^7\text{Be}$ could not be separated from that of the ground state. We deduced the differential cross sections at each scattering angle after subtracting the contribution from the 2^+ peak. Figure 4 shows experimental differential cross sections thus obtained. We estimated that the absolute magnitude of the cross sections was determined within 20% error and zero degree of scattering angle within an accuracy of 0.3° . Error bars include statistical errors and errors due to a subtraction of the 2^+ state in ${}^{12}\text{C}$.

III. FOLDING MODEL CALCULATIONS

To compare the experimental data with the theory we calculated the differential cross sections by the double-folding model.⁴ Similar to the case for ${}^7\text{Li}$ scattering,^{2,4} a projectile and a target wave function were obtained with the microscopic cluster model, $\alpha + {}^3\text{He}$ for ${}^7\text{Be}$ and 3α for ${}^{12}\text{C}$. For ${}^{12}\text{C}$ details of these wave functions have been described elsewhere.¹⁰ For ${}^7\text{Be}$, intercluster wave functions were calculated in the orthogonality condition model (OCM). The nuclear potential parameters used in the OCM calculation are the same as those for the ${}^7\text{Li}$ case.⁴ The calculated wave functions were found to reproduce observed binding energies, energy levels, and $\alpha + {}^3\text{He}$ scattering phase shifts well, and gave reasonable agreement with calculated results of the ground state root-mean-square charge radius, $B(E\lambda)$ values, and a quadrupole moment by Kajino¹¹ in the resonating group method. From these wave functions nucleon density distributions were calculated microscopically.⁴ By using these density distributions, a projectile-target interaction potential was generated by folding the $M3Y$ effective nucleon-nucleon interaction¹² with the zero-range ex-

change term.⁴ A shape of the potential for the imaginary part was assumed to be the same as that for the real part. Therefore we defined the optical potentials $U(r)$;

$$U(r) = (N_R + iN_I)V(r),$$

where $V(r)$ was the double-folding potential. The normalization factors for the real and imaginary parts of the potential, N_R and N_I , were regarded as adjustable parameters and their values were optimized so as to reproduce the observed elastic scattering cross section.

On the other side, in the coupled-channel calculations including the projectile breakup processes, diagonal and coupling potentials were calculated according to the CDCC framework,⁴ where the lowest four channels of the $\frac{3}{2}^-$, $\frac{1}{2}^-$, $\frac{5}{2}^-$, and $\frac{7}{2}^-$ states in ${}^7\text{Be}$ and the ground state of ${}^{12}\text{C}$ were coupled. Here, we neglected the target excitations as well as the nonresonant breakup processes of ${}^7\text{Be}$ because these effects were expected to be not so large^{2,13} on the elastic scattering.

Since the ground state and the $\frac{1}{2}^-$ state at $E_x = 0.43$ MeV in ${}^7\text{Be}$ are experimentally unseparated according to an insufficient energy resolution, the cross section of the $\frac{1}{2}^-$ state was separately calculated in the CDCC framework⁴ and added to a cross section of elastic scattering at each angle. We note that the CDCC calculation is found to reproduce the inelastic cross section for the ${}^7\text{Li}$ case as shown in Fig. 25(b) of Ref. 4. Figures 3(a) and 3(b) show the calculated results of the double-folding and the CDCC models, respectively.

IV. DISCUSSION AND CONCLUSION

It is found that the experimental data are well fitted by the double-folding calculation with $N_R = 0.75$ and $N_I = 0.53$, as shown in Fig. 3(a). A large reduction of 25% in the real potential strength is necessary to fit the data. This large reduction is not dependent on the shape of the imaginary potential; even by using a Woods-Saxon shape for the imaginary potential, experimental data are also fitted only with the real normalization factor of 0.75. This amount of the large reduction is also seen in the case of ${}^6,{}^7\text{Li}$ scattering.^{2,4}

On the other hand, as shown in Fig. 3(b), experimental data are also well reproduced by the coupled-channel calculation. It is noted that the normalization factors for the real and imaginary potentials are $N_R = 1.0$ and $N_I = 0.4$, respectively. Therefore we found that no reduction in the real potential strength is necessary in this calculation. The origin of the reduction of the potential strength in the double-folding analysis is clearly found to be attributed to the projectile breakup processes.

From this result, we conclude that in the present ${}^7\text{Be}$ scattering the projectile breakup effect induces a repulsive real potential with a strength of 0.25 times the double-folding potential, similar to the case for ${}^6,{}^7\text{Li}$.

This experiment was performed at the Research Center for Nuclear Physics, Osaka University under Program Nos. 25A08, 25C08, and 26A23.

-
- ¹I. Tanihata, H. Hamagaki, O. Hashimoto, Y. Shida, N. Yoshikawa, K. Sugimoto, O. Yamakawa, T. Kobayashi, and N. Takahashi, *Phys. Rev. Lett.* **55**, 2676 (1985).
²K. Katori, T. Shimoda, T. Fukuda, S. Shimoura, A. Sakaguchi, M. Tanaka, T. Yamagata, N. Takahashi, H. Ogata, M. Kamimura, and Y. Sakuragi, *Nucl. Phys.* **A480**, 323 (1988), and references therein.
³I. J. Thompson and M. A. Nagarajan, *Phys. Lett.* **106B**, 163 (1981).
⁴Y. Sakuragi, M. Yahiro, and M. Kamimura, *Prog. Theor. Phys. Suppl.* **89**, 136 (1986); Y. Sakuragi, *Phys. Rev. C* **35**, 2161 (1987).
⁵G. R. Satchler and W. G. Love, *Phys. Rep.* **55**, 183 (1979).
⁶R. S. Mackintosh and A. M. Kobos, *Phys. Lett.* **116B**, 95 (1982); Y. Sakuragi, M. Yahiro, and M. Kamimura, *Prog. Theor. Phys.* **70**, 1047 (1983).
⁷M. Tanaka, T. Yamagata, S. Nakayama, M. Inoue, Y. Sakuragi, M. Kamimura, K. Goto, K. Katori, M. Yanagi, and H.

- Ogata, *Phys. Rev. C* **36**, 2146 (1987); M. Tanaka, T. Yamagata, S. Nakayama, M. Inoue, K. Goto, K. Katori, M. Yanagi, and H. Ogata, *Nucl. Instrum. Methods A* **267**, 139 (1988).
⁸S. Nakayama, T. Yamagata, K. Yuasa, M. Tanaka, M. Inoue, T. Itahashi, and H. Ogata, *Phys. Rev. C* **34**, 366 (1986); *Phys. Lett. B* **195**, 316 (1987).
⁹T. Noro, T. Takayama, H. Ikegami, M. Nakamura, H. Sakaguchi, H. Sakamoto, H. Ogawa, M. Yosoi, T. Ichihara, N. Isshiki, M. Ieiri, Y. Takeuchi, H. Togawa, T. Tsutsumi, and S. Kobayashi, *Suppl. J. Phys. Soc. Jpn.* **55**, 470 (1986).
¹⁰Y. Fukushima and M. Kamimura (unpublished); M. Kamimura, *Nucl. Phys.* **A351**, 456 (1981).
¹¹T. Kajino, *Nucl. Phys.* **A413**, 323 (1984), and private communication.
¹²G. Bertsch, J. Borysowicz, H. McManus, and W. G. Love, *Nucl. Phys.* **A284**, 399 (1977).
¹³Y. Sakuragi, M. Kamimura, and K. Katori, *Phys. Lett. B* **205**, 204 (1988).